Bulg. J. Phys. **45** (2018) 54–66

Photon Beam Fluence and Energy at the Phantom Surface as a Function of Primary Electron Energy: Monte Carlo Study Using BEAMnrc Code, DOSXYZnrc and BEAMDP Code

M. Bencheikh, A. Maghnouj, J. Tajmouati
LISTA Laboratory, Physics Department, Faculty of Sciences Dhar El-Mahraz, University of Sidi Mohamed Ben Abdellah, Fez, Morocco

Received *18 September 2017*

Abstract. The purpose of this study is to provide detailed characteristics of incident photon beams for different primary electron energy for the field size of 10×10 cm^2 in terms of the photon fluence profile, energy photon fluence profile, and energy photon distribution, The method used in this study was the Monte Carlo calculation method, it is considered to be the most accurate method for dose calculation in radiotherapy. The Monte Carlo codes used were the BEAMnrc code to simulate the 6 MV photon beam produced by Varian Clinac 2100 and photon transport, DOSXYZnrc code to simulate the absorbed dose in a water phantom, and the BEAMDP for the photon beam characteristics at the surface water phantom. We have calculated the percentage depth dose (PDDs) for the 10×10 cm^2 field size and the calculated PDDs was compared to the measured PDD, and the gamma index was determined as a function of depth in the phantom, the gamma index criterions used was 3% for dose difference and 3 mm for distance to agreement.

The acceptance criterion was more than 95% and the statistical uncertainty was 1%. The photon beam characteristic maximum increased in a linear manner as a function of the primary electron energy. The percentage of the beam characteristic maximum was determined relative to the primary electron energy of 6.1 MeV. For example, for a primary electron energy of 6.7 MeV, the percentage of the photon fluence maximum was 23.22% of the photon fluence maximum at 6.1 MeV, the percentage of the photon energy fluence maximum was 32.69% of the photon energy fluence maximum at 6.1 MeV, and the percentage of the photon energy distribution maximum was 19.39% of the photon energy distribution maximum at 6.1 MeV. Our study can be useful to improve photon beam dosimetry and radiotherapy quality.

PACS codes: 87.50.cm, 87.10.Rt, 87.50.st

1 Introduction

Medical linear accelerators (Linac) are widely used in modern radiotherapy, due to their flexibility and their high therapeutic reliability. The photon beam is produced by energetic electrons striking a target generally constructed of tungsten due to its high atomic number to facilitate the production of photons by bremsstrahlung [1-3]. In this study, the calculation method was the Monte Carlo method; the Monte Carlo methods have been used extensively in medical physics for modeling linear accelerators and for radiation therapy calculations. The Monte Carlo methods used are considered the most accurate method for predicting dose distributions for treatment-planning purposes [8-31].

Several possible approaches are described and discussed in detail in previous publications. One approach of a source model is to characterize the beam analytically, as described by Jiang et al. [45], Another approach is to perform complete Monte Carlo simulations of the radiation transport through the accelerator head [38-44]. In this study, the Monte Carlo codes used were the BEAMnrc to simulate the linac head; this code provides the phase space (PS) files [33]; the BEAMDP was used to analyze the phase space files (PSF) for determining the photon beam characterization at the water phantom surface. The DOSXYZnrc was used to simulate the photon beam transport in the water phantom and to calculate the dose within the water phantom [34]. The STATEDOSE code to read and to analyze .3ddose files output of DOSXYZnrc and to make the necessary operations on dose calculation distribution in the phantom including the dose normalization to maximum dose [47].

The geometry Monte Carlo of 6 MV photon beam produced by Varian Clinac 2100 was built with BEAMnrc based on manufacturer-provided information (Varian Medical System); the field size was 10×10 cm^2 and the distance source surface (SSD) was 100 cm. The physical process was modelled according to EGSnrc code, wherein we have simulated the transport of radiation as realistically as possible [35]. The PSF was generated by the BEAMnrc code that contains the necessary data (position, momentum, energy, and charge) for all particles traversing the phase space scoring plane. The PSF were used in BEAMDP code, in order to analyze the PSF data in terms of photon fluence profile, photon energy fluence profile, and photon energy fluence distribution. The PS plane was at the water phantom surface (on Z axis $z = 100$ cm). Based on the PSF, the photon beam characterization was analyzed, the primary electron energy varied from 6.1 to 6.7 MeV with 0.2 MeV step. This study represents an investigation of the photon beam characteristic sensitivity to primary electron energy for a purpose to contribute in the linac dosimetry improvement and in the electron source above the target refinement.

The measured percentage depth dose (PDD) was performed for Varian Clinac 2100 linear accelerator, the beam energy is 6 MV for the open field size of

10×10 cm^2, and the SSD is 100 cm. All the reference PDD measurements were performed using a motorized scanning system in a PTW. The simulation validation of Varian Clinac 2100 was performed using the gamma index method as a technique for the quantitative evaluation of dose distribution comparison as Low et al. [20,46]. The gamma index criterions were choose as used in the work of Palta et al. [4] and they set to allow the dose difference (DD) and distance to agreement (DTA) of 3% and 3 mm respectively. The gamma index acceptance rate was almost 99% for percentage depth dose (PDD), and almost 98% for beam dose profiles, thus, the Varian Clinac 2100 Monte Carlo geometry was validated according the tolerance limit recommended by TRS430 [5] and in IAEA-TECDOC-1583 [6].

2 Materials and Methods

2.1 Monte Carlo simulation validation

For Monte Carlo simulation validation of 6 MV photon beam produced by Varian Clinac 2100, the gamma index values, which were ≤ 1, defined the agreement between the measured and the calculated dose distribution along the depth in the water phantom, and the gamma index acceptance rate was determined.

Figures 1 and 2 show the PDD distribution comparison and gamma index evaluation, and dose profile comparison and gamma index evaluation, respectively for the field size of 10×10 cm^2, the photon beam energy of 6 MV and SSD of 100 cm.

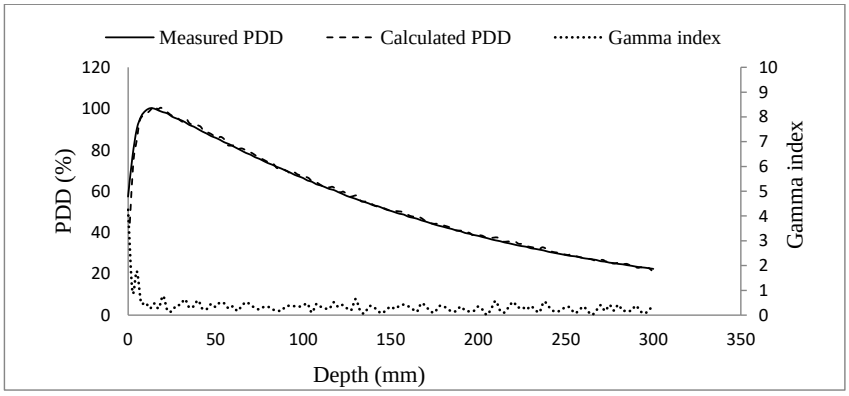

Figure 1. Measured PDD, calculated PDD, and gamma index as a function of depth on the beam central axis in the water phantom. The 6 MV photon beam produced by Varian Clinac 2100, the field size was 10×10 cm^2 and the SSD was 100 cm.

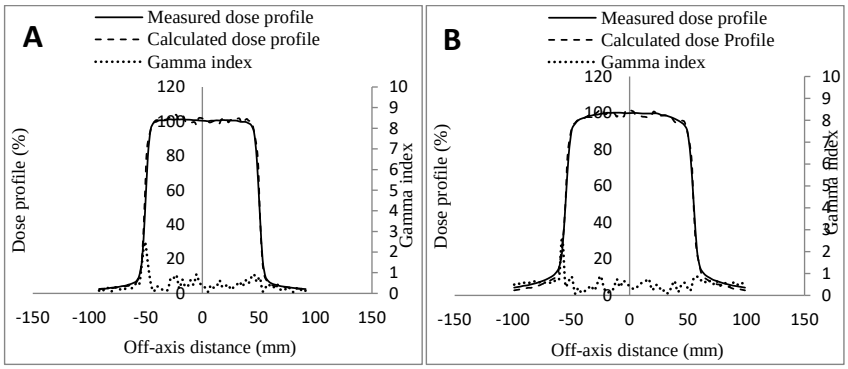

Figure 2. Measured dose profile, calculated dose profile, and gamma index as a function of off axis distance at: a depth of $D_{\max}$ (A); and a depth of 10 cm (B) on the beam central axis in the water phantom. The 6 MV photon beam produced by Varian Clinac 2100, the field size was 10×10 cm^2 and the SSD was 100 cm.

The gamma index acceptance rate was 99 % for the criteria (3%/3mm) for the PDD distribution; in the next, the Monte Carlo simulation was validated for the dose profiles at a depth of maximum dose ($D_{\max}$) and at a depth of 10 cm, the field size was 10×10 cm^2.

The gamma index passing rate was found for the criteria (3%, 3 mm) at 97% for the dose profile distribution at a depth of $D_{\max}$ and 98,62% for the dose profile distribution at a depth of 10 cm, thus the Varian Clinac 2100 Monte Carlo simulation was validated with accuracy and as realistically as possible. Our results revealed that the PDDs and beam profiles agreed by almost 99% and 97%, respectively, and within the tolerance limit recommended by TRS430 [5] and in IAEA-TECDOC-1583 [6]. The gamma index found marked a good and more developed calculation in comparison with previous study as it was done by Kadman et al. [7].

For the validated Monte Carlo simulation, the primary electron source above the target was elliptical form and it had the Gaussian spread. Its characterizations were X- and Y-coordinates equal to 1.4 mm, the mean angle spread of primary electrons was 1° and the electron source energy was 6.52 MeV.

2.2 Primary electron assumptions

The initial electron energy is not clearly provided by the manufacturer and varies among linacs of the same model [17-21,24]. Based on the primary electron energy validated above, the electron beam energy was selected surrounding the energy validated of 6.52 MeV. The Monte Carlo calculation was performed for a monodirectional electron point source upon the target and the electron energies varied from 6.1 to 6.7 MeV with 0.2 MeV step, and the PDD were calculated,

the results of measurements and calculations were compared to validated within gamma index acceptance rate tolerance of 95%. The gamma index technique was used for the quantitative evaluation for comparing the measured and calculated PDDs, the acceptance gamma index criterions were 3% for the dose deviation (DD) and 3 mm for distance to agreement (DTA).

2.3 PDD validation

The percentage depth dose was validated by acceptance by gamma index criterions; the photon beam characterization was investigated depending on the primary electron energy above the target. The measured PDD and the calculated the PDD were plotted for each value of primary electron energy. Figure 3 presents the measured PDD and the calculated PDDs as a function of depth on the beam central axis for each value of primary electron energy. The field size is 10×10 cm^2, the photon beam energy of 6 MV produced by Varian Clinac 2100, and the SSD is 100 cm. The SP file was recorded at z=100 cm at the water phantom surface and directly under the air gap.

For all primary electron energy, the gamma index was determined to compare the calculated PDDs to measured PDD. Figure 4 presents the gamma index curve as function of depth on the beam central axis. The percentage of acceptance of gamma index criterions was more than 95 % for all primary electron energy studied.

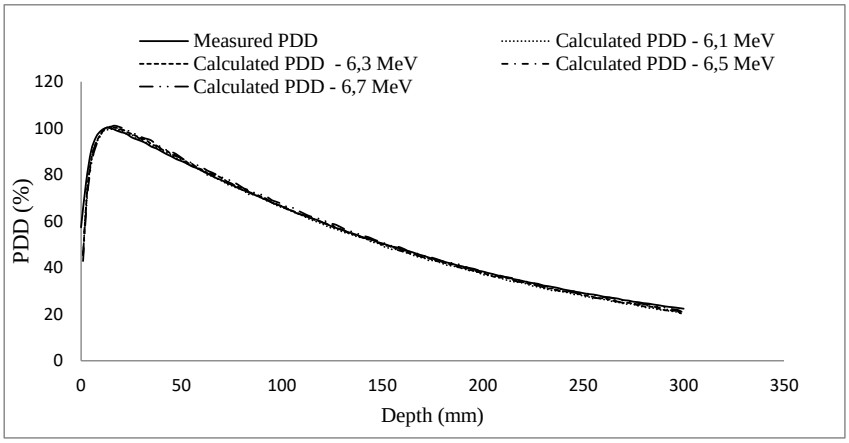

Figure 3. Measured PDD and calculated PDDs as a function of depth in a water phantom on the beam central axis for each value of primary electron energy (6.1 MeV; 6.3 MeV; 6.5 MeV; and 6.7 MeV). The photon beam energy of 6 MV produced by Varian Clinac 2100, the field size is 10×10 cm^2, and the SSD is 100 cm.

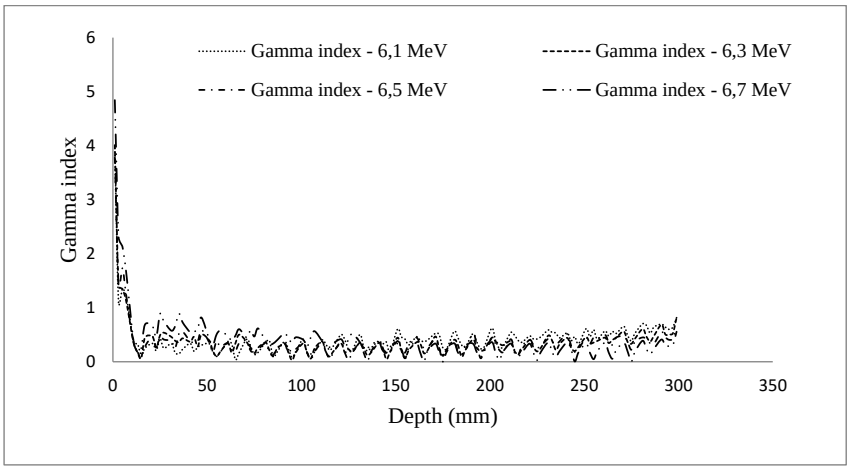

Figure 4. Gamma index as function of depth in water phantom on the beam central axis for each value of primary electron energy (6.1 MeV; 6.3 MeV; 6.5 MeV; and 6.7 MeV).

3 Results and Discussion

3.1 Photon fluence profile

Based on PS file at the water phantom surface, the planar photon fluence profiles were determined as a function of the off axis distance, Figure 5 presents the planar photon fluence profiles for each value of the primary electron energy.

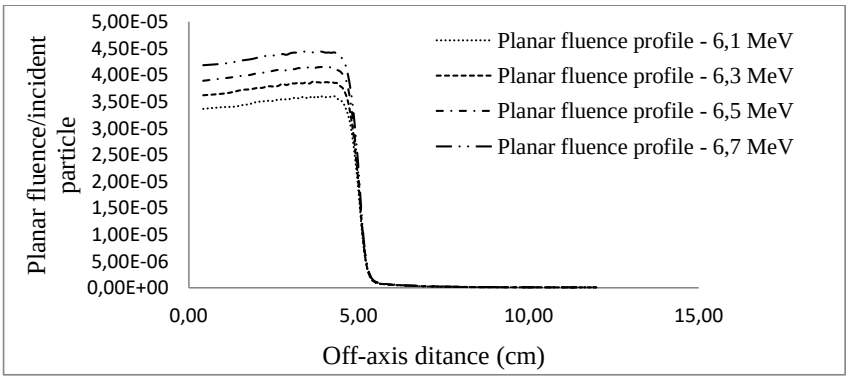

Figure 5. The planar photon fluence profiles as a function of off axis distance at the water phantom surface for a 10×10 cm^2 field size for each value of primary electron energy (6,1 MeV; 6,3 MeV; 6,5 MeV; and 6,7 MeV). The photon beam of 6 MV produced by Varian Clinac 2100 accelerator, and the SSD is 100 cm.

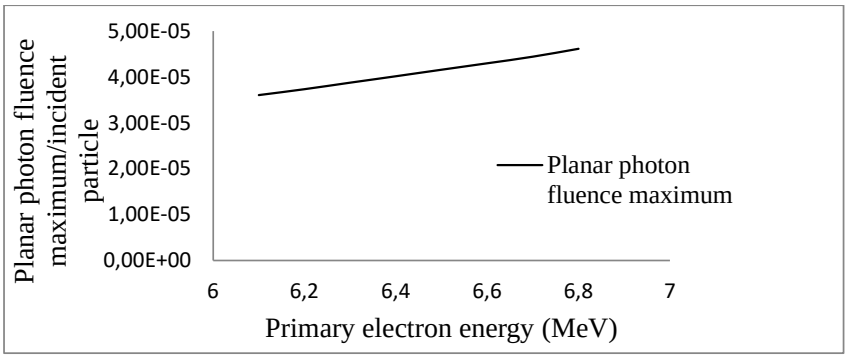

Figure 6. The variation of photon fluence maximum as a function of the primary electron energy at the water phantom surface.

The photon fluence profiles increased with the primary electron energy above the linac target, and the planar photon fluence profiles kept the same difference between them in the off-axis range from 0 to 5 cm and all planar photon fluence profiles have zero at the beam edge.

It can be seen that the photon fluence maximum for each planar photon fluence profile increased with the primary electron energy and moved in the increasing primary electron energy in a linear manner. For this purpose, the photon fluence profile maximum was determined for each planar photon fluence curve, and Figure 6 shows the variation of photon fluence profile maximum as a function of the primary electron energy above the linac target.

The photon fluence profile maximum varied in a linear manner as a function of the primary electron energy and the slope of the line was 1,285 10^{-05} photon per incident particle per MeV. The photon fluence maximum increased with increasing of primary energy electron above the target.

3.2 Photon energy fluence profile

The photon energy fluence has an interesting role in dosimetry study of external radiotherapy and in deep tumor treatment [1-5,47]. The energy fluence profiles were determined as a function of off-axis distance. Figure 7 gives the photon energy fluence profiles for each value of the primary electron energy.

The photon energy fluence profiles increased with the primary electron energy above the target, and the planar photon fluence profiles kept the same difference between them in off-axis range from 0 to beam edge (almost at 5 cm) and all planar photon energy fluence profiles have zero at the beam edge.

It can be seen that the photon energy fluence maximum for each planar photon energy fluence profiles increased with the primary electron energy and moved in

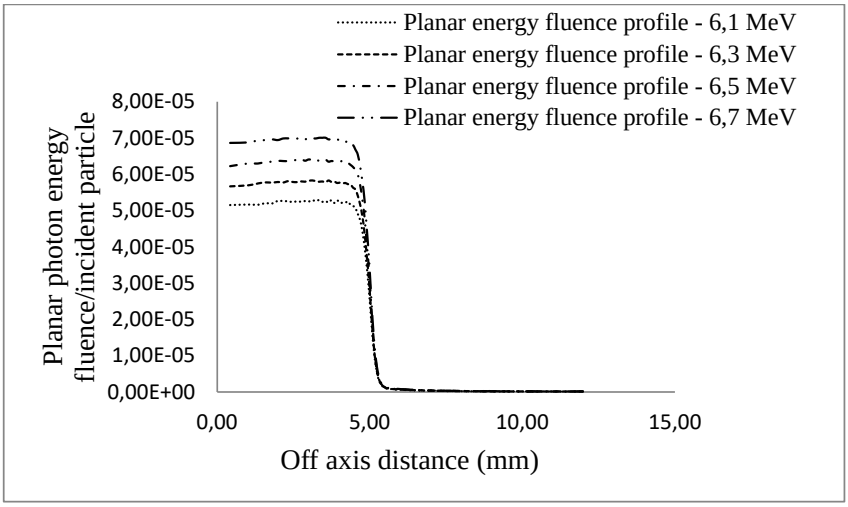

Figure 7. The planar photon energy fluence profiles as a function of off axis distance at the water phantom surface for a 10×10 cm^2 field size for each value of primary electron energy (6.1 MeV; 6.3 MeV; 6.5 MeV; and 6.7 MeV). The photon beam of 6 MV produced by Varian Clinac 2100 accelerator, and the SSD is.100 cm.

the increasing primary electron energy in a linear manner. The photon energy fluence maximum varied depending on the primary electron energy above the target. Figure 8 presents the photon energy fluence maximum as a function of the primary electron energy.

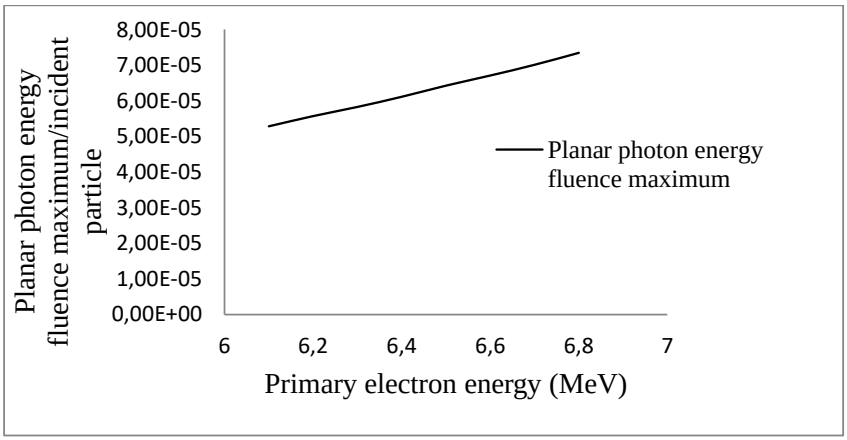

Figure 8. The variation of the photon energy fluence maximum as a function of the primary electron energy at the water phantom surface.

The photon energy fluence maximum varied in a linear manner as a function of the primary electron energy and the slope of the line was 2,861 10^{-05} MeV per incident particle per MeV

3.3 Photon energy fluence distribution

We have investigated also the energy fluence distribution depending on the primary electron energy above the Varian Clinac 2100 target. Figure 9 shows the variation of the energy fluence distribution as a function of the energy.

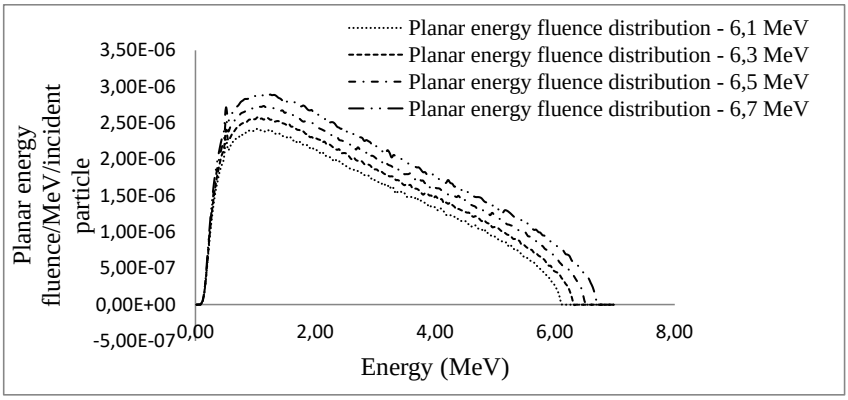

Figure 9. The planar photon energy fluence distributions as a function of the energy at the water phantom surface for a 10×10 cm^2 field size for each value of primary electron energy (6,1 MeV; 6,3 MeV; 6,5 MeV; and 6,7 MeV). The photon beam of 6 MV produced by Varian Clinac 2100 accelerator, and the SSD is 100 cm.

The photon energy fluence distribution increased with the increasing of primary electron energy above the target, and the photon fluence distribution kept the same difference between them in the energy range from 0.5 MeV to 6 MeV, and the most of the photons have an energy of 1.24 MeV.

It can be seen that the photon energy fluence maximum for each photon energy fluence distribution increases with increasing of primary electron energy and moved in the increasing primary electron energy as a linear manner. The photon energy fluence maximum varied depending on the primary electron energy above the target. Figure 10 presents the photon energy fluence maximum distribution as a function of the primary electron energy.

The planar photon energy fluence distribution maximum varied in a linear manner as a function of the primary electron energy and the slope of the line was 6,49 10^{-07} MeV per incident particle per MeV.

It can be seen from Figure 5, Figure 7, and Figure 9, the photon fluence profile, the photon energy fluence profile and the photon energy fluence distribution

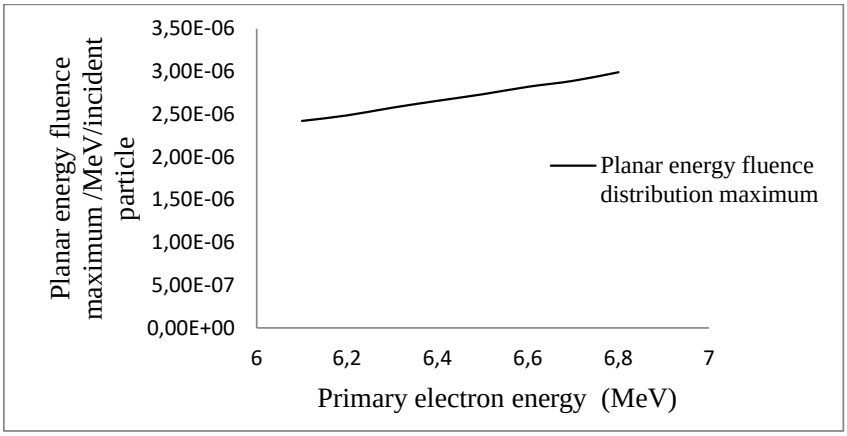

Figure 10. The variation of photon energy distribution maximum as a function of the primary electron energy at the water phantom surface.

increased with increasing of primary electron energy. To illustrate the primary electron energy effects on the photon beam characterizations, we have calculated the deviation characterization quantity maximum relative to those of 6.1 MeV as formula below:

$$\text{Deviation} = 100 \times \frac{\text{Max}(X_{\text{primary electron energy}}) - \text{Max}(X_{6,1})}{\text{Max}(X_{6,1})}, \qquad (1)$$

where X: phhoton characterization quantity at the photon surface.

Figure 11 presents the variation of deviation of photon beam characterization maximum relative to photon beam characterization at primary electron energy 6.1 MeV as a function of the primary electron energy.

The photon energy fluence maximum increased more than both photon fluence maximum and energy fluence distribution maximum as a function of the primary electron energy. For primary electron energy at 6.7 MeV, the percentage of photon fluence maximum was 23.22% of photon fluence maximum at 6.1 MeV, the percentage of photon energy fluence maximum was 32.69% of photon energy fluence maximum at 6.1 MeV, and the percentage of photon energy distribution maximum was 19.39% of photon energy distribution maximum at 6.1 MeV.

The photon energy maximum increased as a function of the primary electron that striking the target for producing the photons by bremsstrahlung effects and the photon energy varied up to the electron energy above the target. Our study illustrates the relationship between the both variations of photon fluence and photon energy fluence as function of the primary electron energy above the Varian Clinac 2100 target using the Monte Carlo method.

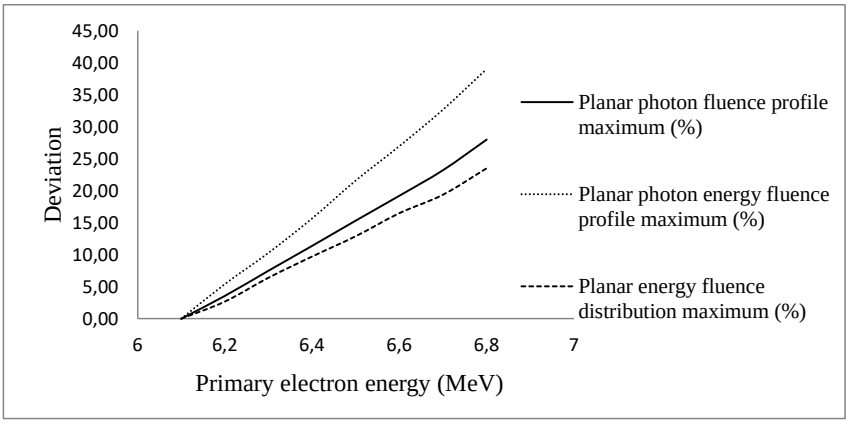

Figure 11. Variation percentage of photon fluence maximum relative to photon fluence maximum at 6.1 MeV, the percentage of photon energy fluence maximum relative to photon energy fluence maximum at 6.1 MeV, and the percentage of photon energy distribution maximum relative to photon energy distribution maximum at 6.1 MeV as a function of the primary electron energy.

3.4 The statistical uncertainty

The statistical uncertainty of Monte Carlo simulation of 6 MV photon beam produced by Varian Clinac 2100 was 1 at the maximum dose as found by M. Aljamal et al. [40].

4 Conclusion

This study presents an investigation on the primary electron energy on the photon beam characterization at the water phantom surface, according to photon beam characterization required; the primary electron energy above the target was selected, this study also illustrates that optimal beams will have high fluence and low energy fluence that recommended by IAEA in TRS-398 [49].

The variation of photon fluence, photon energy fluence, and photon energy fluence distribution were varied in a linear manner depending on the primary electron energy [9]. Our study can be useful to improve photon beam dosimetry, radiotherapy treatment and to design new accelerators more efficient and of high quality in the photon external beam radiotherapy; the optimal photon beam can be found as high photon fluence and low photon energy fluence to save the healthy cells surrounding the tumor volume treatment [5].

Acknowledgement

The authors would like to thank VARIAN Medical Systems to provide us the Varian Clinac 2100 geometry data and give us this opportunity to study the VARIAN linear accelerator technology and to participate in its future development, our study is one among many study over the world in this field.

References

[1] P. Mayles, A. Nahum, and J.C. Rosenwald (2007) "*Handbook of Radiotherapy Physics Theory and Practice*" (Taylor & Francis group, LCC, USA) pp. 452-480.

[2] D.S. Chang, F.D. Lasley, I.J. Das, M.S. Mendonca, and J.R. Dynlacht (2014) "*Basic Radiotherapy Physics and Biology*" (Springer, New York) pp 77-92.

[3] E.B. Podgorsak (2005) "*Radiation Oncology Physics: A Handbook for Teachers and Students*" (IAEA, Vienna) pp 161-216.

[4] J. Palta, S. Kim, J. Li, and C. Liu (2003) In: "*Intensity-Modulated Radiation Therapy: The State of the Art*", Proceeding of the AAPM 2003 Summer School, eds. J.R. Palta and T.R. Mackie (Madison, WI: Medical Physics) pp 593-612.

[5] Technical Reports Series No.430 (2004) Commissioning and Quality Assurance of Computerized Planning Systems for Radiation Treatment of Cancer (IAEA, Vienna).

[6] IAEA-TECDOC-1540 (2007) Specification and Acceptance Testing of Radiotherapy Treatment Planning Systems (IAEA, Vienna).

[7] B. Kadman, N. Chawapun, S. Ua-Apisitwong, T. Asakit, N. Chumpu, and J. Rueansri (2016,*J. Phys. Conf. Ser.* **694** 012023.

[8] D.M. Lovelock, C.S. Chui, and R. Mohan (1995) *Med. Phys*. **22** 1387-1394.

[9] H.H. Liu, T.R. Mackie, and E.C. McCullough (1997) *Med. Phys*. **24** 1960-1974.

[10] B. Libby, J. Siebers, and R. Mohan (1999) *Med. Phys*. **26** 1476-1483.

[11] C.M. Ma, E. Mok, A. Kapur, T. Pawlicki, D. Findley, S. Brain, K. Forster, and A.L. Boyer (1999) *Med. Phys*. **26** 2133-2143.

[12] A.E. Schach von Wittenau, L.J. Cox, P.M. Bergstrom, W.P. Chandler, C.L. Hartmann Siantar, and R. Mohan (1999) *Med. Phys*. **26** 1196-2110.

[13] J.V. Siebers, P.J. Keall, B. Libby, and R. Mohan (1999) *Phys. Med. Biol*. **44** 3009-3026.

[14] I. Chetty, J.J. DeMarco, and T.D. Solberg (2000) *Med. Phys*. **27** 166-172.

[15] S.B. Jiang, A. Kapur, J. Li, T. Pawlicki, and C.M. Ma (2000) *Phys. Med. Biol*. **45** 411-427.

[16] W. Van der Zee, and J. Welleweerd (1999) *Med. Phys*. **26** 1883-1892.

[17] C.M. Ma (1998) *Radiat. Phys. Chem*. **53** 329-344.

[18] M.K. Fix, H. Keller, P. Ruegsegger, and E.J. Born (2000) *Med. Phys*. **27** 2739-2747.

[19] M.K. Fix, M. Stampanoni, P. Manser, E.J. Born, R. Mini, and P. Ruegsegger (2001) *Phys. Med. Biol*. **46** 1407-1427.

[20] D.A. Low, J.F. Dempsey (2003) *Med. Phys.* **30** 2455-2464.

[21] M.K. Fix, P.J. Keall, K. Dawson, and J.V. Siebers (2004) *Med. Phys*. **31** 3106-3121.

[22] C.L. Hartmann Siantar, R.S. Walling, T.P. Daly, B. Faddegon, N. Albright, P. Bergstrom, A.F. Bielajew, C. Chuang, D. Garrett, R.K. House, D. Knapp, D.J. Wieczorek, and L.J. Verhey (2001) *Med. Phys*. **28** 1322-1337.

[23] P. Francescon, C. Cavedon, S. Reccanello, and S. Cora (2000) *Med. Phys*. **27** 1579-1587.

[24] D. Sheikh-Bagheri, D.W. Rogers (2002) *Med. Phys*. **29** 391-402.

[25] P.J. Keall, J.V. Siebers, B. Libby, and R. Mohan (2003) *Med. Phys*. **30** 574-582.

[26] R.D. Lewis, S.J. Ryde, D.A. Hancock, and C.J. Evans (1999) *Phys. Med. Biol*. **44** 1219-1230.

[27] B.T. Sichani and M. Sohrabpour (2004) *Phys. Med. Biol*. **49** 807-818.

[28] M. Dumitrache and A. Tanase (2012) A Comparative Study On 6 MV Photon Beam Percentage Depth Dose Of VARIAN Clinac 2300 C/D, ELEKTA Synergy Platform, and Siemens Primus Linacs, Sofia, European Medical Physics and Engineering Conference, October 18-20.

[29] R. Popa, M. Dumitrache, and A. Ciovlica (2012) *Rom. Rep. Phys.* **64** 997-1010.

[30] A. Mesbahi, P. Mehnati, and A. Keshtkar (2007) *Iran. J. Radiat. Res.* 23-30.

[31] A. Mesbahi, M. Fix, M. Allahverdi, E. Grein, and H. Garaati (2005) *Appl. Radiat. Isot.* **62** 469-477.

[32] L. Apipunyasopon, S. Srisatit, and N. Phaisangittisakul (2013) *J. Radiat. Res.* **54** 374-382.

[33] D.W.O. Rogers, B. Walters, and I. Kawrakow (2013) "em BEAMnrc Users Manual" (NRCC Report, Ottawa) pp 12-254.

[34] B. Walters, I. Kawrakow, and D.W.O. Rogers (2013) "*DOSXYZnrc Users Manual* (NRCC Report, Ottawa) pp 9-103.

[35] D.W.O. Rogers, I. Kawrakow, J.P. Seuntjens, B. Walters, and H.E. Mainegra (2013) "*NRC User Codes for EGSnrc*" (NRCC Report, Ottawa) pp 6-83.

[36] C.M. Ma and D.W.O. Rogers (2013) "*BEAMDP Users Manual*" (National Research Council of Canada, NRCC Report, Ottawa) pp 3-24.

[37] M. Asghar, M. Parinaz, K. Ahmad, F. Alireza (2007) *Radiat. Med.* **25** 315-324.

[38] J.K. Paul, V.S. Jeffrey, L. Bruce, and M. Radhe (2003) *Med. Phys*. **30** 574-582.

[39] A. Mesbahi (2006) *Iran. J. Radiat. Res*. **4** 7-14.

[40] D. Sheikh-Bagheri and D.W. Rogers (2002) *Med. Phys*. **29** 379-390.

[41] M. Oprea, C. Constantin, D. Mihailescu, C. Borcia (2012) *U.P.B. Sci. Bull. Ser. A* **74** 153-166.

[42] F. Verhaegen, J. Seuntjens (2003) *Phys. Med. Biol.* **48** 3401-58.

[43] K. Aljarrah, G.C. Sharp, T. Neicu, and S.B. Jiang (2006) *Med. Phys.* **33** 850-858.

[44] O. Chibani, B. Moftah, C.M. Ma (2011) *Med. Phys.* **38** 188-201.

[45] S.B. Jiang, A.L. Boyer, and C.M. Ma (2001) *Med. Phys.* **28** 55-66.

[46] D.A. Low, W.B. Harms, S. Mutic, and J.A. Purdy (1998) *Med. Phys.* **25** 656-661.

[47] H.C.E. McGowan, B.A. Faddegon, and C.M. Ma (2013) STATDOSE for 3D dose distributions (NRCC Report, Ottawa) pp 1-10.

[48] M. Aljamal and A. Zakaria (2013) *Aust. J. Basic Appl. Sci.* **7** 340-346.

[49] IAEA (2000) Absorbed dose determination in external beam radiotherapy (Technical reports series no. 398, Vienna) pp 110-133.